RESEARCH INSTITUTE FOR HIGH ENERGY PHYSICS

REPORT SERIES

The Results of the Combined Beam Test of the DELPHI Hadron Calorimeter, the Forward Electromagnetic Calorimeter and the Barrel Muon Chambers, (π^+, e^+ Runs)

H. Herr, A. M. Wetherell, G. Zumerle
CERN

G. D. Alekseev, V. M. Golovatyuk, R. B. Kadyrov, N. Khovansky,
G. V. Mitselmakher, J. Ridky, G. Shelkov, V. Timofeev,
E. N. Tsyganov, V. Vrba
JINR Dubna

P. Eerola, R. Keränen, R. Lauhakangas, J. Pyyhtiä,
R. Orava, M. Voutilainen
University of Helsinki

I. Lippi, M. Mazzucato
INFN Padova

C. Bosio, E. Graziani
INFN Sanita

E. Chernyaev, P. V. Chliapnikov, A. B. Fenyuk, V. V. Lapin,
V. I. Nikolaenko, S. A. Gumenyuk, V. F. Obraztsov, A. M. Zaitsev
IHEP Serpukhov

CSEFT

THE RESULTS OF THE COMBINED BEAM TEST OF THE DELPHI HADRON CALORIMETER, THE FORWARD ELECTROMAGNETIC CALORIMETER AND THE BARREL MUON CHAMBERS, (π^+, e^+ RUNS)

H.Herr, A.M.Wetherell, G.Zumerle
CERN

G.D.Alekseev, V.M.Golovatyuk, R.B.Kadyrov,
N. Khovansky, G.V.Mitselmakher, J.Ridky, G.Shelkov,
V.Timofeev, E.N.Tsyganov, V.Vrba
JINR Dubna

P.Eerola, R.Keränen, R.Lauhakangas, J.Pyyhtiä,
R.Orava, M.Voutilainen
University of Helsinki

I.Lippi, M.Mazzucato
INFN Padova

C.Bosio. E.Graziani
INFN Sanita

E.Chernyaev. P.V.Chliapnikov. A.B.Fenyuk. V.V.Lapin,
V.l.Nikolaenko, S.A.Gumenyuk,
V.F.Obraztsov, A.M.Zaitsev
IHEP Serpukhov

Abstract

The responses of the DELPHI Hadron Calorimeter (HCAL) and the DELPHI Forward Electromagnetic Calorimeter (FEMC) are investigated in the beam test setup which realizes the actual foreseen DELPHI geometry and data acquisition system. Samples of pion and positron data in the momentum interval $10 - 60$ GeV/c are collected from which the responses of the HCAL, the FEMC and their combined response are analyzed. For the bare HCAL, the response to hadrons is linear in the considered momentum interval. The energy signal ratio of pions and electrons (π/e) is equal to 0.7. The hadronic energy resolution does not scale with $1/\sqrt{E}$ and the mechanisms affecting the energy resolution are studied. Calibration constants are defined for the FEMC and the HCAL separately and the combined response to hadrons is analyzed. Electron separation from pions is studied by using the FEMC and the combined information.

1   Introduction

During July and August 1988, modules of the DELPHI Endcap Hadron Calorimeter (HCAL), the Forward Electromagnetic Calorimeter (FEMC) and the Barrel Muon Detector (MUB) were tested in the H6 beam in the North Area at CERN (Figure 1). In the present report the results concerning the combined analysis of the pion and positron data using the HCAL and the FEMC are considered. The results of the muon runs together with a detailed description of the MUB are presented in the separate paper [1].

2   The Apparatus

2.1   Hadron Calorimeter

The DELPHI HCAL [2] is an iron sampling calorimeter, with limited streamer mode detectors. It consists of a barrel part with 24 modules and two endcaps with 12 sectors. The geometry of the detector is shown in Figure 2 a). The sector number 5 from the end-cap face C (positive z-hemisphere in the standard DELPHI coordinates) was used in this experiment (Figure 2b)). In DELPHI the inner and outer parts of the HCAL sectors are self-supporting, so special flanges were designed to connect the parts together for this experiment.

The detector elements are eight-cell (cell size $9 \times 9\ mm^2$) plastic streamer tubes with a graphite cathode. Each detector plane is covered with a capacitive copper clad read-out board which is subdivided into pads. Corresponding pads of four sequential planes (seven for the first layer) are connected in the signal read-out and form projective read-out towers. The geometry of one of the detector planes in the end-plug part of the module which was actually used is shown in Figure 2b). The detectors are parallel to the outer edge of the calorimeter for even planes end to the inner edge for odd ones, resulting in triangular dead spaces at the edges.

The standard gas mixture composed of Argon : Isobutane : CO_2 in the ratio 1 : 3 : 6 and the voltage of 3.9 kV were used in the HCAL. The high voltage and gas flow of the calorimeter was switched on for two months in total and operated very stably. The NA32 and NA12 experiments were also taking data during this period and due to this there was a high muon background flux of 1 particle/$s\ cm^2$ all over the surface of the calorimeter. In a special run the HCAL module was exposed to a high flux of muons $\sim 10^5$ particles/$s\ m^2$. During this run the total current in the high voltage system of the HCAL was 50 μA ($2\mu A$ being a nominal value). These

1

background conditions are well above those expected for DELPHI. No dark current problems (from which the prototypes of the HCAL had suffered) were found in any of these conditions, due to the improved design of the final version of the streamer tubes.

The final DELPHI Hadron Calorimeter front-end electronics [3] was used with the amplification factor of 10 pC/ADC-count. Because the BCO signal (time of beam crossing over) is needed in the read-out cycle of the HCAL front-end electronics, it was impossible to use an external trigger to start the charge collection (there was a 500 ns unavoidable delay between the external trigger and the actual start of the integration which would lead to a complete loss of signal). This is why a timing configuration, similar to that of the DELPHI cosmic trigger, was used. The resulting scheme is presented in Figure 4 in which the trigger signal and instruction cable delays are taken into account. The cycle was started by sending the start-charge-collection (SCC) instruction randomly. The gate for external trigger was set to 1 μs and was initialised about 300 ns before the start of the charge collection. In case there was a trigger, the read-out cycle was started, otherwise the reset instruction was sent which took 4 μs. So, the HCAL was sensitive only 1/6 of the full time. The time to collect charge for the trigger and data was 300 − 1000 ns and 1300 − 2000 ns respectively from the passage of a particle through the calorimeter. In order to simulate the LEP conditions in an adequate way a very short trigger gate (i.e. a low trigger efficiency) should have been used, but this was impossible because of the low hadron beam intensity. Therefore, the timing used was a reasonable compromise and its effects on the data sample will be discussed in the following chapters.

2.2   The Forward Electromagnetic Calorimeter

The DELPHI Forward Electromagnetic Calorimeter [4] consists of two 5 m diameter disks with a total of 9064 lead glass blocks in form of truncated pyramids, dealigned for ($-3°$) towards the interaction point. For this test, the module #432 was used. It contained 80 lead glass blocks arranged in a rectangular 8×10 matrix. It was positioned in such a way to have the beam hitting one of the central counters with the direction parallel to the block axis.

The standard electronics chain [5] was used for the read-out giving an average noise per counter equivalent to 17 MeV of deposited electromagnetic energy.

2

2.3 The data acquisition system

The data was transferred from the front-end electronics to FASTBUS crates. The structure of the system is shown in Figure 5.

The interface module FRC which can receive data from 8 front-end crates was used in the HCAL. The data was transferred through a special auxiliary bus to another FASTBUS card, the HFB which is a ring buffer and it can have up to four events in memory. The next stage of the data acquisition is the FIP (Fast Intersegment Processor), which uses the 68020 processor and the OS-9 operating system. When the FIP has read an event it sends a message to the LES (Local Event Supervisor, in the GPM processor) which reads the data as a master. The FASTBUS system was interfaced with a μVAX-II through a CFI module. In the VAX each run was stored on the disk and consequently copied on the tape.

3 The test beam

The experiment was carried out in the H6 tertiary test beam of CERN North Area. The beam was tuned to the momenta 10, 20, 40, 60 GeV/c with $\Delta p/p = 1\%$. The momentum of the H6 secondary beam was fixed to 200 GeV/c.

The tertiary pion flux varied from 10 pions/burst for the 10 GeV/c beam to 100 pions/burst for 60 GeV/c (burst length 1.4 s). The muon contamination was high: it was of the order of 50% of the hadron flux over the area of 15×15 cm^2 at the high momenta and increased to 200% for 10 GeV/c. Therefore the value of 10 GeV/c was a difficult point and practically the lowest possible for the H6 beam. The positron flux was significantly higher than the hadron one, 50 positrons/burst at 10 GeV/c and 300 positrons/burst at 60 GeV/c.

The beam trigger included coincidence of two scintillators (10×10 cm^2 and 2×2 cm^2) in front of the FEMC and two CEDARs (differential Cherenkov counters) 90 m upstream. For pion runs the CEDARs were tuned for the pion selection, and in addition a lead plate of $4\,mm$ in thickness was used to suppress the positron background. For the positron runs the lead plate was removed and the CEDARs were tuned accordingly. The dark points marked 1,2,3,4 on Figure 3 correspond to the beam image at the entrance of the layers 1,2,3,4 of the HCAL. The beam was not perpendicular to the HCAL surface ($\cos\theta = 0.4$) in order to reproduce the DELPHI projective geometry.

4 Summary of the data samples

The data can be subdivided into two parts: the 'bare HCAL data', during which there was no FEMC in the beam, and 'the combined data', during which the FEMC was upstream of HCAL. Both sets of data consist of runs with π^+ (e^+) momenta 10, 20, 40 and 60 GeV/c. In addition to this data, separate runs were taken with a different current in the vertically bending magnet in front of the test area, in order to scan the HCAL module in ϕ direction. The FEMC was not in the beam during these runs. The summary of runs is presented in Table 1.

The data processing consisted of the decoding of the information and tests of the data format. The search and the rejection of the repeated events was performed. This was necessary, because this experiment was the first one where the DELPHI data acquisition system was tested. The percentage of 'bad' events was 3-5 %.

As it was already mentioned, the samples contained significant muon background which had to be rejected at the analysis level. For this purpose the information from the Muon Detector was used to veto the event - that is, the events with one good penetrating track were rejected. In addition, internal HCAL criteria (a muon like signal in 3 out of 4 superlayers) were used to suppress further the muon background.

5 The response of the HCAL

5.1 Hadronic response

Figure 6 presents the distributions of the response of the HCAL to 10, 20, 40 and 60 GeV/c pions. The energy dependence is presented in Figure 7. A linear fit $ADC = \alpha \times P + \beta$ gives $\alpha = 5.04 \pm 0.32, \beta = 1.61 \pm 9.1$ with $\chi^2 = 0.55$, (2 D.O.F). The linear response is in contradiction with the results reported in the prototype tests [6,7]. The most probable explanation is the different gas mixture Argon:Isobutane: $CO_2 = 1 : 3 : 6$ instead of Argon:Isobutane=1:3 which results in a smaller streamer charge and in smaller dead zones around the streamer.

The measured energy resolutions are summarized in Table 2a). The resolution expected for a hadron calorimeter with the 5 cm iron slots is [8] $\sigma(E)/E \simeq 0.9/E^{1/2} \left[GeV^{1/2} \right]$ which was confirmed by the HCAL prototype data. The following aspects can explain the worse resolution found in the present experiment:

1. Detector effects: The beam entered in the HCAL in the area of

distributed dead regions due to the streamer tube configuration at the edge of the module (Figure 3). Thus, the sampling of active detector layers was effectively reduced. Secondly, the charge diffusion (i.e. the phenomenon of longitudinal spread of the streamer charge on the cathodes onto several neighbouring pads which was observed in the end-cap module, see discussion in [1]) possibly affected the resolution. For the high momentum data, the leak of energy outside the calorimeter could play a role.

These effects were carefully studied by the DELSIM32 Monte Carlo simulation program [9] which takes into account dead zones as well as other known effects: the electronics threshold, the charge diffusion etc. The result is shown in Table 2b). The deviation from the naive $\sigma(E)/E = 0.9/E^{1/2} \left[GeV^{1/2}\right]$ prediction is distinguishable. In order to check the simulation, the resolution for a barrel point having no dead zones was determined and the results are presented in Table 2c). There is a good agreement with the $\sim 0.9/E^{1/2}$ dependence in the range that has been tested by the prototypes $(3 - 10\ GeV/c)$. In order to test further the simulation program, the experimental longitudinal profiles of 20 GeV/c pion induced showers were compared with the Monte Carlo prediction (Figure 8). The comparison is absolute, that is, the relative normalization was not tuned.

As it is seen from Tables 2 a)-c), the simulation gives qualitative explanation of the data (worsening of the resolution and its deviation from $\sim 1/E^{1/2}$ dependence), but there is still a discrepancy of about 20%.

2. There is a specific effect present in the HFM experiment which can affect the resolution: Because of the non existence of the BCO signal for the read-out cycle of the HCAL front-end electronics, a cosmics-type random-start trigger was used (see Figure 4). The charge integration was started 300 ns after the beginning of the pretrigger gate (see the dashed area in Figure 4), thus some fraction of charge might be lost for the 'early' particles. The effect was estimated using the muon runs in [1]). It can reach 20% level.

3. Worth mentioning is also the variation of the distance between the foil which covers the detector plane from the side, opposite to the pads and the detector plane. According to [10], a variation of $\sim 1\ mm$, which is quite possible, can lead to the 10% variation in response.

5

In summary, we achieved a qualitative explanation of the lower resolution seen in this test. The main effects are specific to the HFM experimental arrangement and they vanish in the region below 10 GeV.

5.2 The calibration of the HCAL

Because the channel-to-channel variations in the HCAL response (due to the dead zones etc.) can be responsible for the smearing of the signal, there was a hope to improve the resolution of the HCAL by using a calibration procedure. The most simple way would be to use muons for this purpose. For example, one can select the events, where a muon crosses the center of the given tower, and use the inverse of the average charge in the tower as the calibration coefficient. However, our numerous attempts to calibrate the HCAL by using the muons failed. The main reason for this is the charge diffusion phenomenon together with relatively high thresholds in the front-end electronics. The charge diffusion implies that the average charge in the central tower, under conditions described above, is about 15 pC instead of 50 pC in the absence of the diffusion. On the other hand, the uncertainty in the front-end threshold is about 10 pC, thus it is impossible to distinguish the threshold variation effect from the difference of the response of channels to the deposited energy. This is, in fact, the most serious problem which has been discovered during the test and which can effect the performance of the HCAL during the real data taking.

The most straightforward way to improve the situation would be to increase the sensitivity of the front-end electronics (a factor of 2 would be enough) and to adjust accurately the pedestals with potentiometers. As this is not realistic for the first data taking periods of the LEP, it is also possible to measure on-line the front-end thresholds for all the channels (the ADC-writing level signal can be used for this purpose). By using a random trigger and by moving the writing level one can define the point where the pedestal noise appeares in a given channel.

As the muon calibration turned out to be impossible, we tried the direct hadron calibration. The idea was to minimize the functional $\sum_i \left(\sum_k \left(c_k A_k^i - E_{\text{beam}} \right)^2 \right)$ where i is an event number, k is a tower index, A_k^i is the charge in the tower k in the event i; c_k is a calibration coefficient. The procedure is rather complicated, because the total number of towers involved in the showers is $\sim 80 - 90$. Two technically different approaches were used: a) minimization using the MINUIT program [11] and b) the use of an iterative procedure. Figure 9 gives the distribution of the coefficients. The improvement in the resolution of HCAL can be seen by comparing

Table 2a) and Table 3.

5.3 The response of the HCAL to positrons

The collected samples of positron data make it possible to study the HCAL response to positrons. This is important, because in some DELPHI regions HCAL is the only calorimeter. The ratio π/e is measured to be 0.707 and 0.730 for 10 GeV/c and 20 GeV/c, respectively (see Figure 7). So the calorimeter is undercompensated. The energy resolution of the HCAL is 28% for 10 − 20 GeV/c positrons.

5.4 Test of the HCAL trigger chain

One of the functions of the HCAL in DELPHI is to provide muon and hadron trigger. For this purpose, the HCAL raw data contains the digitized total analog charge sum for each half-sector. This charge is digitized $1\mu s$ before the tower data. The scatter plot of the off-line sum of the charge in the sector versus the trigger sum is displayed in Figure 10. The linear behaviour of the analog sum confirms the proper operation of the trigger chain. Moreover, taking into account the pedestal in the analog sum distribution, both off-line and analog charge distributions have the same relative width.

6 The FEMC response to positrons

Processing of the FEMC data consisted of the pedestal subtraction for each cell and the multiplying on the calibration coefficient. Both sets of constants were determined in the separate FEMC calibration in the North Area. However, the amplification and timing of the shaper cards used in this test were different from the ones used in the FEMC calibration runs. The main effect was corrected comparing the electronic test pulses in the two different conditions. The residual miscalibration is of the order of 2-3%. No special effort was done to correct for this effect because the optimization of the energy resolution was outside the scope of this test. In order to eliminate the pedestal fluctuations, the threshold of 20 MeV was introduced for each channel. To minimize the effect of electronics noise, only cells in 3 × 3 matrix around the cell with maximum signal were taken into account. The total calibrated signal from the FEMC is presented in Figure 11 for 10, 20 and 40 GeV/c positron beam. The energy resolution can be approximated by $\sigma(E)/E = 9\%/E^{1/2} \left[GeV^{1/2} \right]$.

7 The combined response of the FEMC and the HCAL

7.1 The combined hadronic response

Satisfactory measurements of the hadron energy in DELPHI can be achieved only using combined information from the hadron calorimeter and the electromagnetic detector. One of the main goals of the HFM test was to demonstrate the possibility of the combined calorimetry. For this purpose, runs of 10, 20 and 40 GeV/c pion beam with a module of the FEMC standing upstream of the HCAL were processed. The data for 40 GeV are presented in Figure 12. Figure 12a) shows the total calibrated signal from the FEMC. The distribution contains two components: punching through pions which populate the peak at low energy, and showering pions which give a broad distribution. The response of the HCAL (with the common calibration coefficient 0.18 GeV/ADC for all towers) is dramatically different from that of the stand-alone runs (see Figure 12b) and Figure 6c)). The biplot Figure 12c) shows reasonable correlation of responses of both detectors. First, the punching through pions exhibit normal showering in the HCAL (the dark vertical band), for the other hadrons a strong linear correlation of the HCAL and the FEMC responses is seen. The cluster in the left down corner corresponds to the muon background. The sum of the responses of the two detectors is shown in Figure 13a). A clear peak is seen together with a muon background, but the average energy is underestimated (34 GeV instead of 40 GeV). In the events with significant energy deposition in the FEMC, the reconstructed energy is obviously underestimated. The response of the HCAL for the showers starting in the FEMC is also small. The estimate of the energy can be improved if the following algorithm is used:

For the 'punching through region' $(E_{\text{FEMC}} < 2 \, GeV)$

$$E_{\text{tot}} = E_{\text{HCAL}} + 2.0 \, E_{\text{FEMC}} \qquad (1)$$

For the 'FEMC absorbing region' $(E_{\text{HCAL}} < 1.5 \, GeV)$

$$E_{\text{tot}} = E_{\text{HCAL}} + 1.9 \, E_{\text{FEMC}} \qquad (2)$$

For the 'combined region'

$$E_{\text{tot}} = 1.25 \times \left(E_{\text{HCAL}} + E_{\text{FEMC}} \right) \qquad (3)$$

The result is shown in Figure 13b). The resolution determined as $(FWHM/2.36)/ < E >$ is 32% is better than for the HCAL standing

8

alone. The average total reconstructed energies as well as the resolution obtained for the other beam momenta are shown in Table 4.

7.2   The combined electron separation from pions

It is well known that there are two parameters, measured by electromagnetic calorimeters, which contribute to the electron identification - the dispersion of the transverse distribution of the shower and the total energy. The quadratic variance $\left(\sigma_x^2 + \sigma_y^2\right)^{1/2}$ of the shower space distributions, normalized to the FEMC cell dimension, are presented in Figure 14 for 10 GeV/c positrons and pions. The peak at the zero dispersion for pions corresponds to the punching-through hadrons. With a selection $0.25 < \mathrm{disp} < 0.65$ one can achieve the efficiency of 95% for electrons and the rejection factor of ~ 5.7 against hadrons.

If the momentum of the incoming particle is known independently, for example from the tracking system in the magnetic field, a much better discrimination can be reached. Figure 15 presents the biplot for the shower dispersion versus the total energy in the FEMC for 10 GeV/c positrons and pions. By using the same dispersion selection and by requiring $8\ GeV < E_{FEMC} < 11\ GeV$ for the visible energy in the FEMC, the pion suppression factor can be improved up to ~ 60.

It is also important to have a good electron-pion separation without the tracking system, for example, from the points of view of the fast event tagging and the 4th level trigger. This is why the possible contribution of the HCAL in electron identification was studied here. Figure 16 shows the distribution of the ratio of the energy deposited in the HCAL to that of the FEMC for positrons and pions which passed the dispersion selection criterium. A condition $E_{HCAL}/E_{FEMC} < 0.1$ results in the efficiency of 90% for positrons and gives a combined hadron rejection factor of 35.

Acknowledgements

References

[1] E.Veitch et al., Muon Identification Efficiencies from the HFM Experiment, DELPHI 89-57 PHYS 48, (1989).

[2] DELPHI Collaboration, DELPHI Technical Proposal, CERN/ LEPC/ 83-3.

[3] E.Gygi and F.Schneider, The read out electronics of the hadron calorimeter of DELPHI, CERN/EP 0023P, 1986.

[4] P.Checchia et al. Nucl.Inst.Meth. **A275** (1989) 45-58.

[5] G.Barichello et al. Nucl.Inst.Meth. **A254** (1987) 111-117.

[6] G.A. Akopdzhanov et al., Beam Tests of the Delphi Hadron Calorimeter Prototype, IHEP Preprint 86-62, Serpukhov 1986.

[7] A.Baroncelli et al., Performance of an iron sampling Delphi test hadron calorimeter, INFN-ISS 88/1.

[8] R. Wigmans, Nucl. Inst. and Meth. **A259** (1987), 389.

[9] DELPHI Collaboration, DELSIM DELPHI Event Generation and Detector Simulation, DELPHI 89-68 PROG 143, (1989).

[10] Yu.P.Guz et al., Some features of plastic streamer tube operation, IHEP 86-208, Serpukhov, 1986.

[11] MINUIT minimization package, CERN Program Library.

Tables

Beam momentum (GeV/c)	Run conditions			#Events
10	π+	no Femc		896
20	π+	no Femc		20800
40	π+	no Femc		12870
60	π+	no Femc		5280
20	π+	+100 A	1)	2024
20	π+	+50 A	1)	2016
20	π+	+25 A	1)	4000
20	π+	-25 A	1)	4000
20	π+	-50 A	1)	4036
10	π+	Femc		1375
20	π+	Femc		5046
40	π+	Femc		6186
10	e+	Femc		5142
20	e+	Femc		10309
40	e+	Femc		10049

1) Vertical beam bending

Table 1: Summary of the data samples.

a)

Beam momentum	$\sigma / <ADC>$	$\sigma / <ADC> E^{1/2}$
10 GeV/c	36 %	1.14
20 GeV/c	30 %	1.34
40 GeV/c	29 %	1.80
60 GeV/c	29 %	2.24

b)

Beam momentum	$\sigma / <ADC>$	$\sigma / <ADC> E^{1/2}$
10 GeV/c	40 %	1.26
20 GeV/c	40 %	1.79
40 GeV/c	38 %	2.40
60 GeV/c	32 %	2.47

c)

Beam momentum	$\sigma / <ADC>$	$\sigma / <ADC> E^{1/2}$
3 GeV/c	56.7 %	.98
5 GeV/c	41.3 %	.98
7 GeV/c	35.1 %	.93
10 GeV/c	32.0 %	1.0

Table 2: a) The energy resolution of the HCAL (raw data).

b) The Monte Carlo predictions for the energy resolution of the HCAL endcap module (dead-zone region).

c) The Monte Carlo predictions for the HCAL barrel, (dead-zones-free region).

13

Beam momentum	$\sigma / <ADC>$	$\sigma / <ADC> E^{1/2}$
10 GeV/c	38.8 %	1.23
20 GeV/c	30.4 %	1.36
40 GeV/c	27.9 %	1.77
60 GeV/c	24.5 %	1.90

Table 3: The energy resolution of the HCAL, calibrated data.

Beam	E (GeV)	E_c (GeV)	σ / E	$(\sigma / E) \cdot E^{1/2}$
10 GeV/c	7.1	9.5	35 %	1.10
20 GeV/c	16.4	19.2	33 %	1.47
40 GeV/c	35.0	40.7	32 %	2.02

Table 4: The combined resolution of HCAL+FEMC. The 2nd column shows the uncorrected sum of energies in HCAL and in FEMC. E_c is the corrected energy (see the text). Two last columns present the resolution for the corrected energy.

Figure captions

Figure 1. Plan view of the HFM experiment.

Figure 2. a) The Hadron Calorimeter. b) A HCAL endcap sector.

Figure 3. The geometry of a HCAL detector plane. A layer in the end-plug is shown representing the configuration in the even plane; in the odd planes the streamer tubes are parallel with the symmetry axis of the module. The areas outside the rectangular streamer tubes represent the inactive regions. The solid points show the projection of the beam image in the superlayers 1, 2, 3 and 4.

Figure 4. Random start mode for the HCAL front-end electronics. Two cycles are shown: first is an unsuccessful one (no trigger signal within the pretrigger gate), another one is successful.

Figure 5. HFM FASTBUS data acquisition system.

Figure 6. The response of the HCAL to 10, 20, 40, 60 GeV/c pions (for 60 GeV/c also the data with muon background is shown).

Figure 7. Test of the linearity of the HCAL response. The plot gives the most propable values of the uncalibrated HCAL signals as a function of the beam momentum for pions (circles) and positrons (squares).

Figure 8. Longitudinal shower profile for 20 GeV/c pions in the HCAL (shaded histograms). The unshaded histograms correspond to the Monte Carlo predictions.

Figure 9. The distribution of the HCAL calibration coefficients, the total number of coefficients is 119: $< c > = 0.19$; $\sigma_c = 0.09$.

Figure 10. The total off-line ADC sum versus the trigger analog sum in the HCAL for 20 GeV/c pions.

Figure 11. The FEMC response to 10, 20 and 40 GeV/c positrons (calibrated data).

Figure 12. a) The response of the FEMC to 40 GeV/c pions, b) The response of the HCAL to 40 GeV/c pions with FEMC upstream, c) The HCAL signal versus the FEMC signal for 40 GeV/c pions.

Figure 13. a) The sum of energy deposited in the FEMC and in the HCAL for 40 GeV/c pion beam, b) The corrected energy (see the text).

Figure 14. $\left(\sigma_x^2 + \sigma_y^2\right)^{1/2}$ distribution for 10 GeV/c positrons (a) and pions (b) in the FEMC. The horizontal scale is given in the units of the FEMC cell dimension.

Figure 15. The biplot of shower dispersion vs. the total energy for 10 GeV/c a) positrons b) pions.

Figure 16. The ratio of the energy deposited in the HCAL and in the FEMC for 10 GeV/c a) e^+ b) π^+, which passed the dispersion selection.
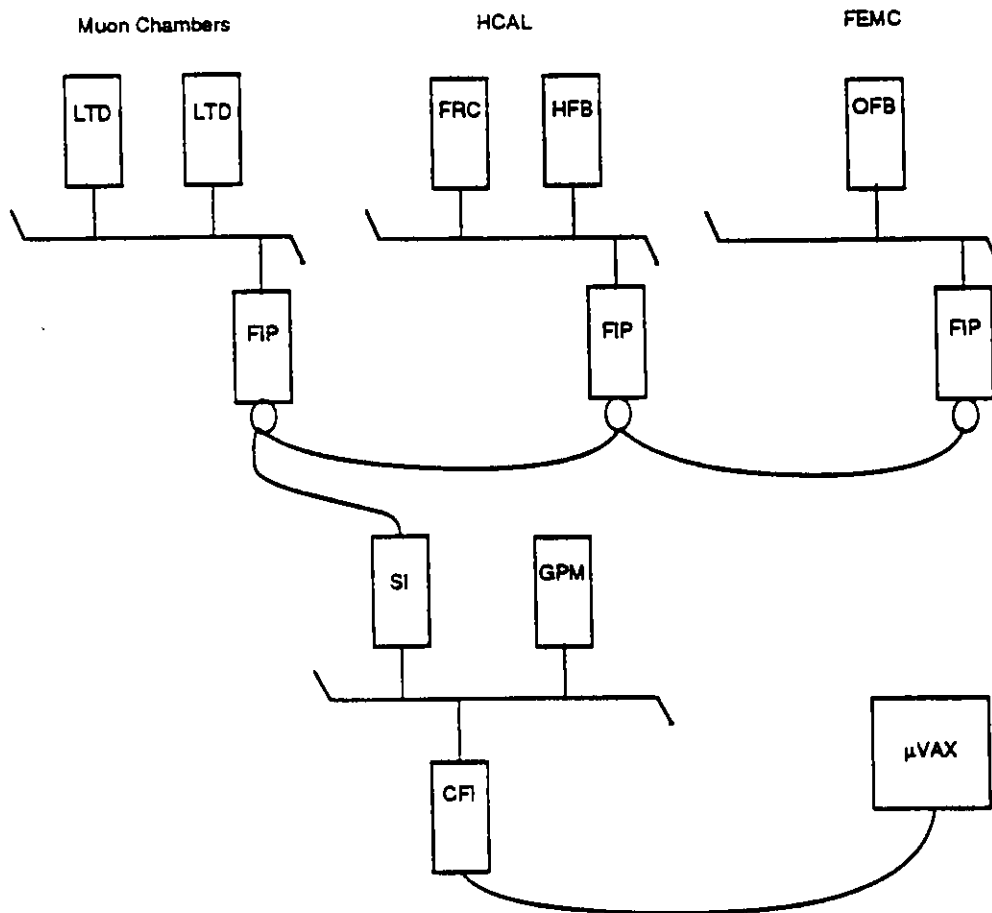
15

Figure 1:

Figure 2:

Figure 3:

Figure 4:

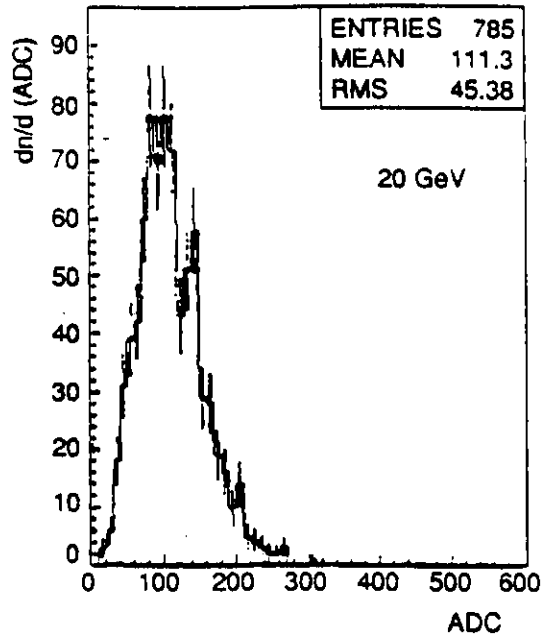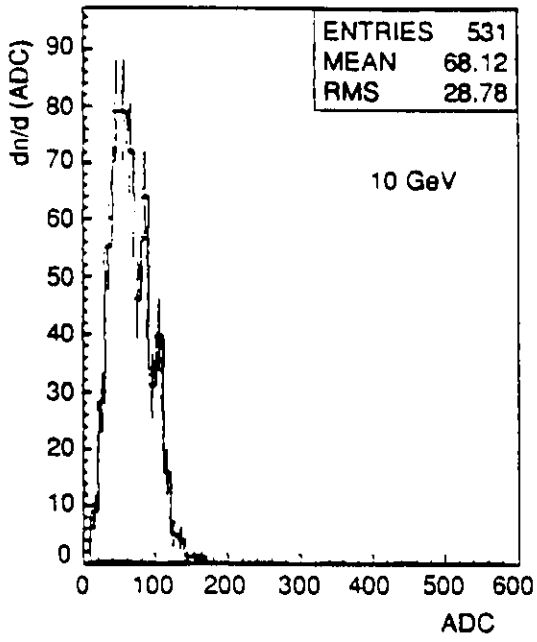Muon Chambers HCAL FEMC

LTD LTD FRC HFB OFB
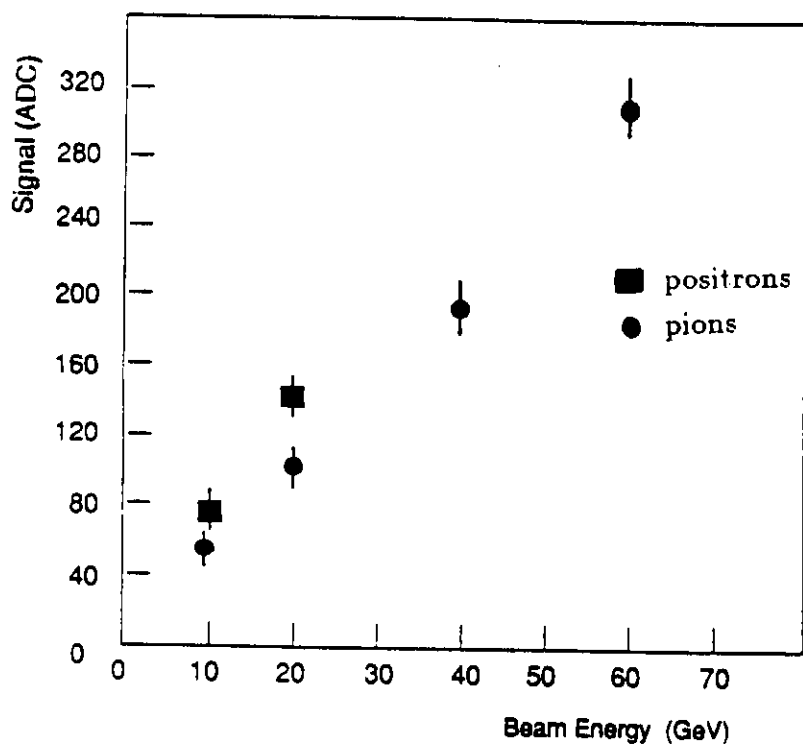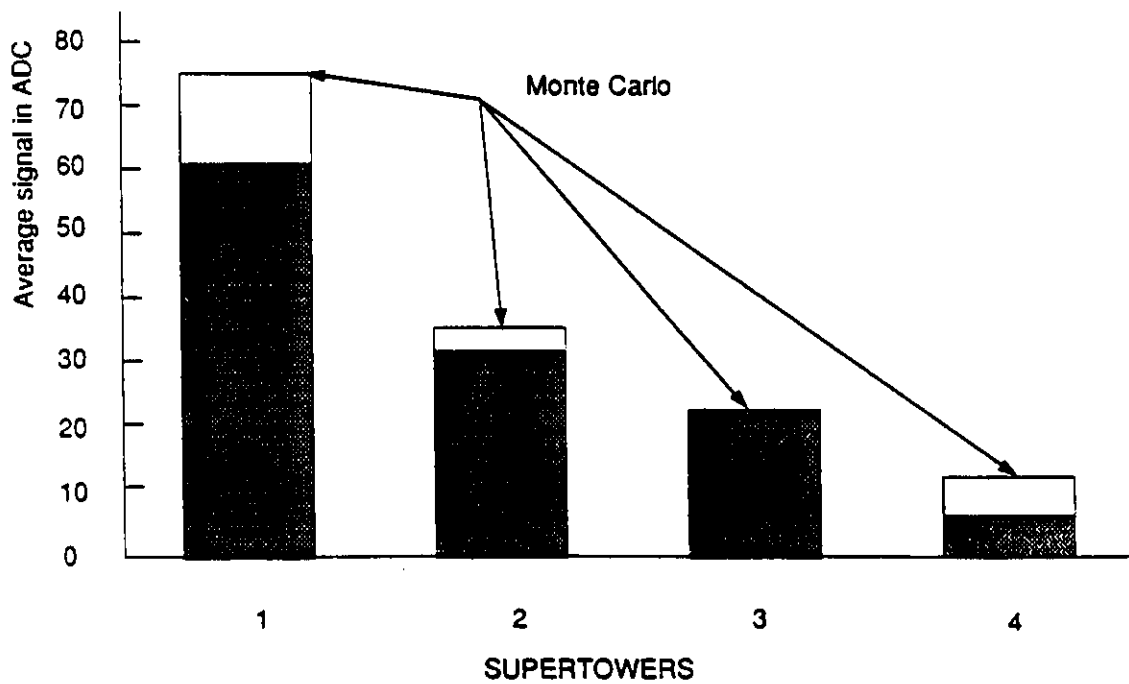
FIP FIP FIP

SI GPM

μVAX

CFI
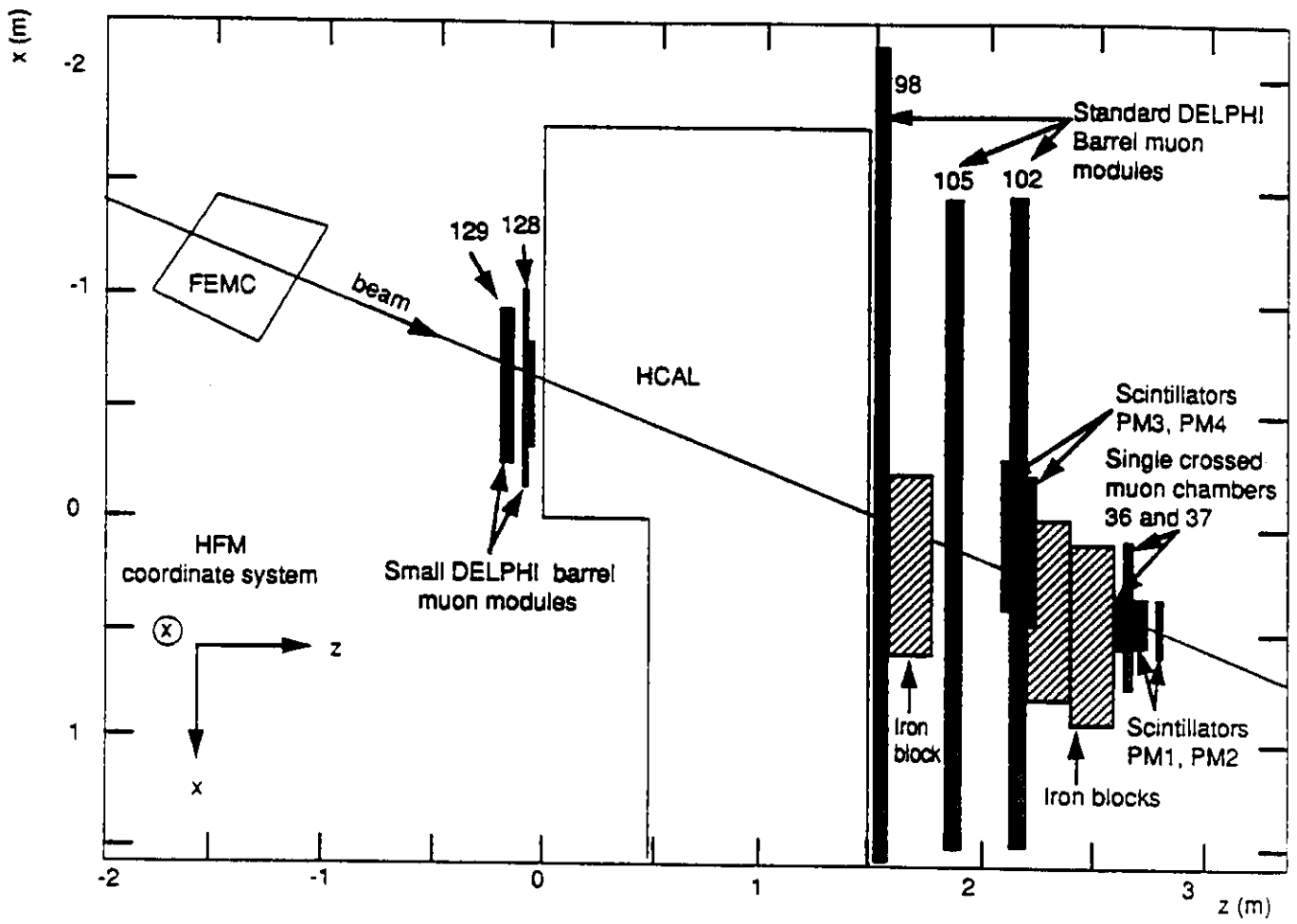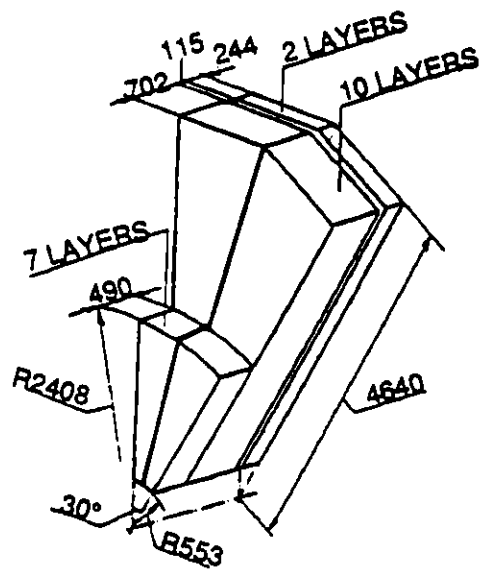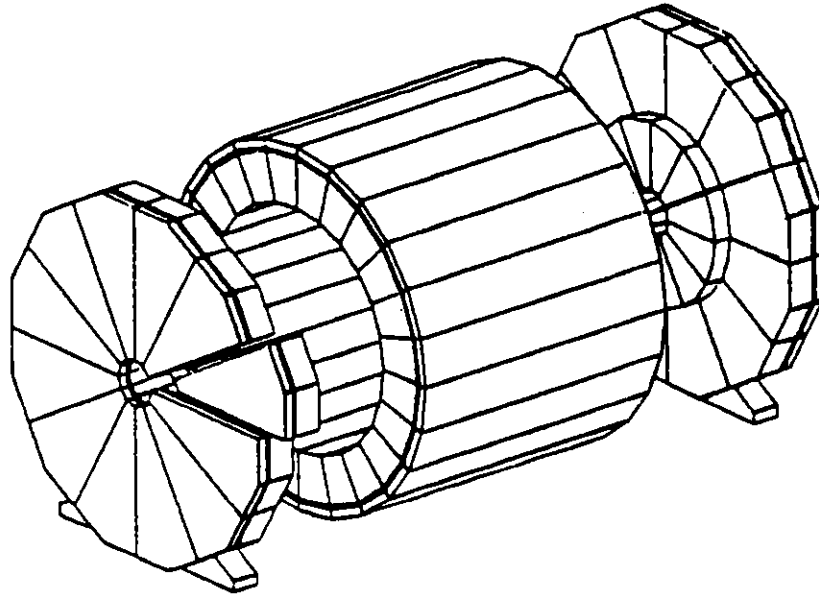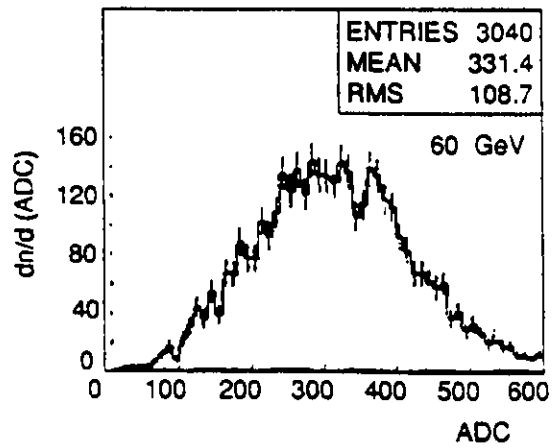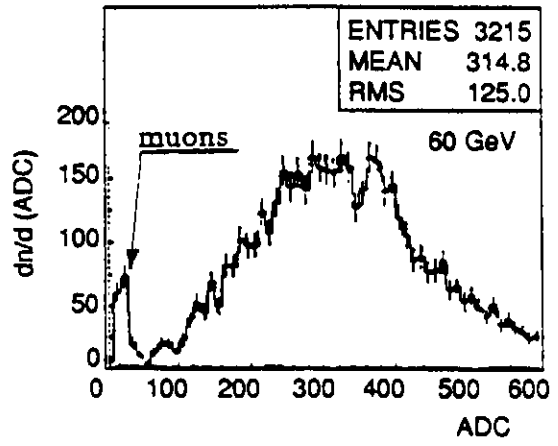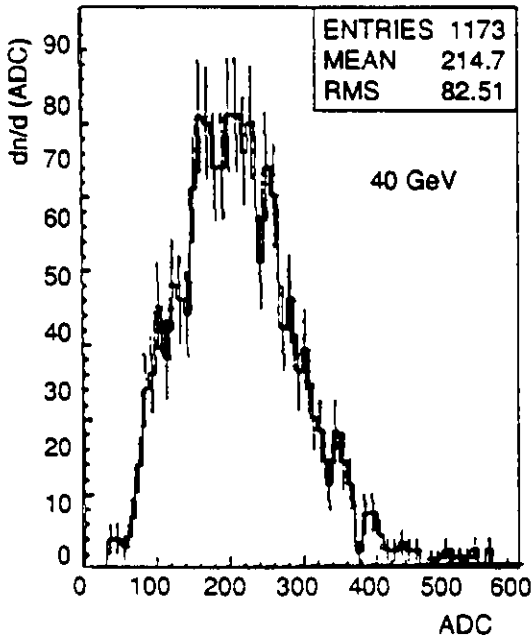
Figure 5:

Figure 6:

Figure 7:

Figure 8:
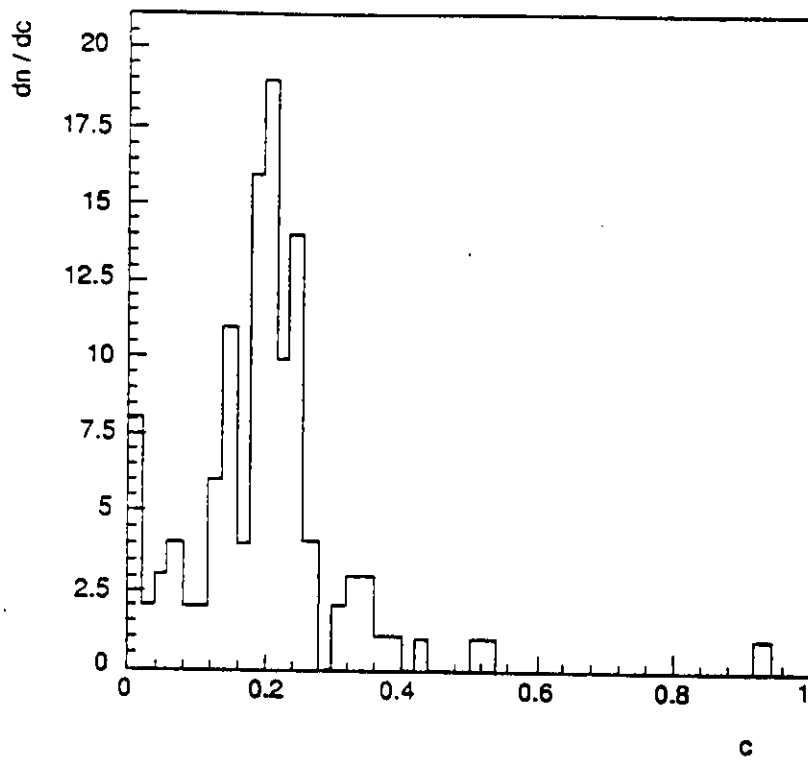
Figure 9:
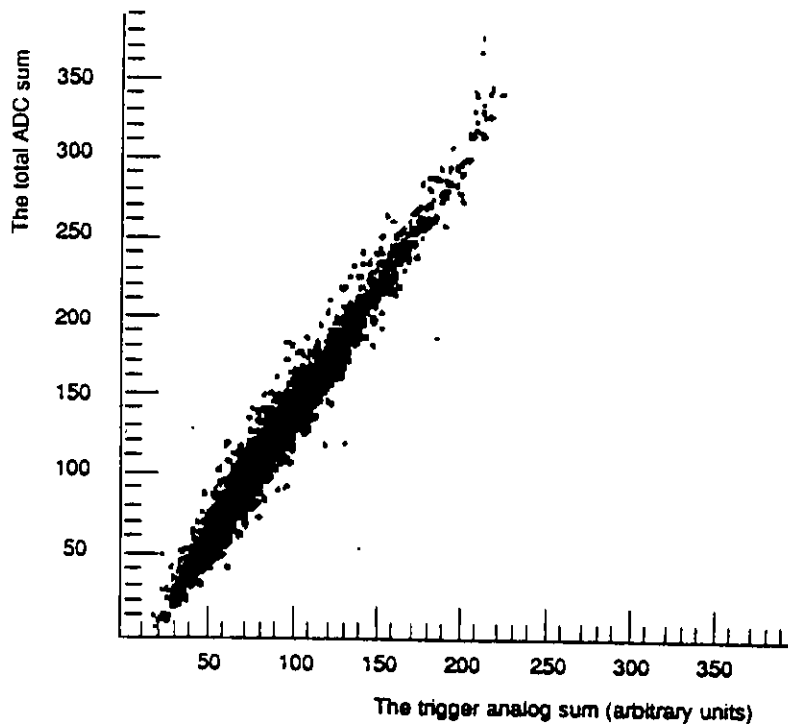
Figure 10:

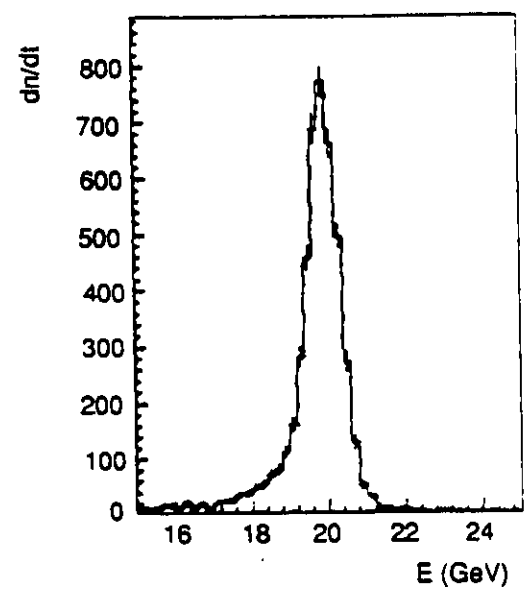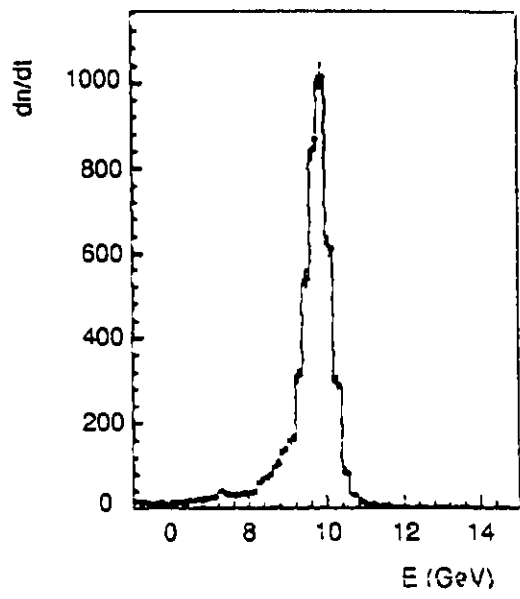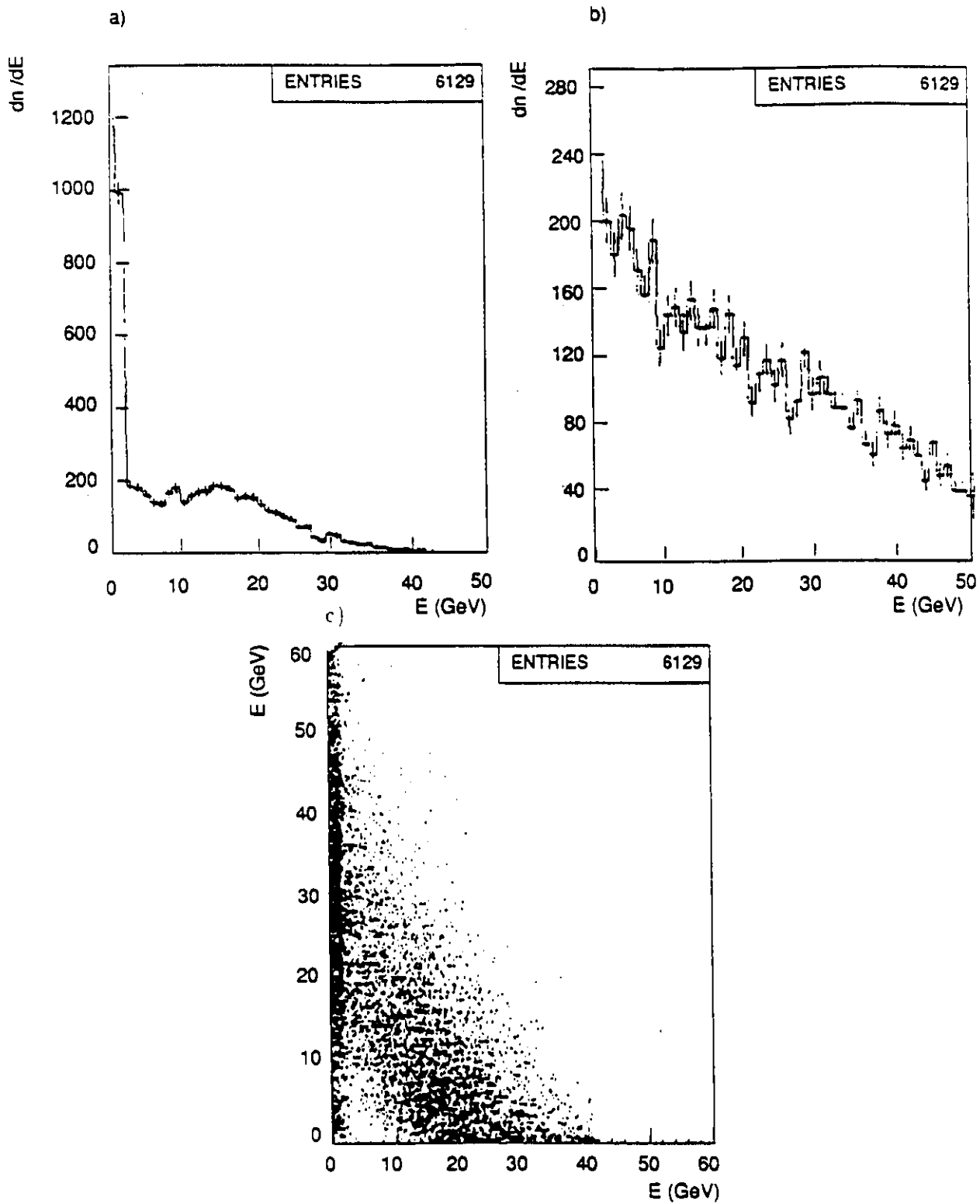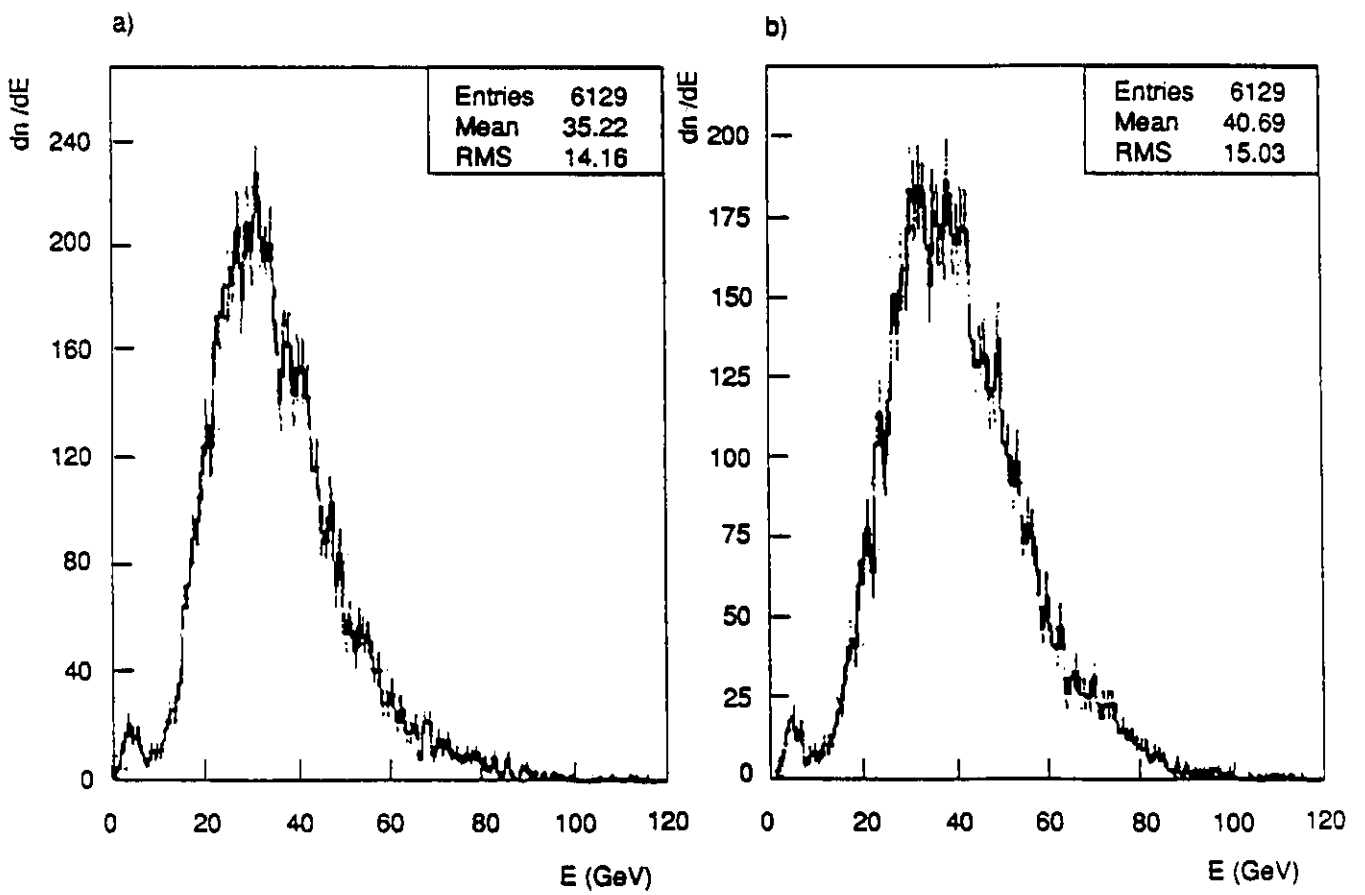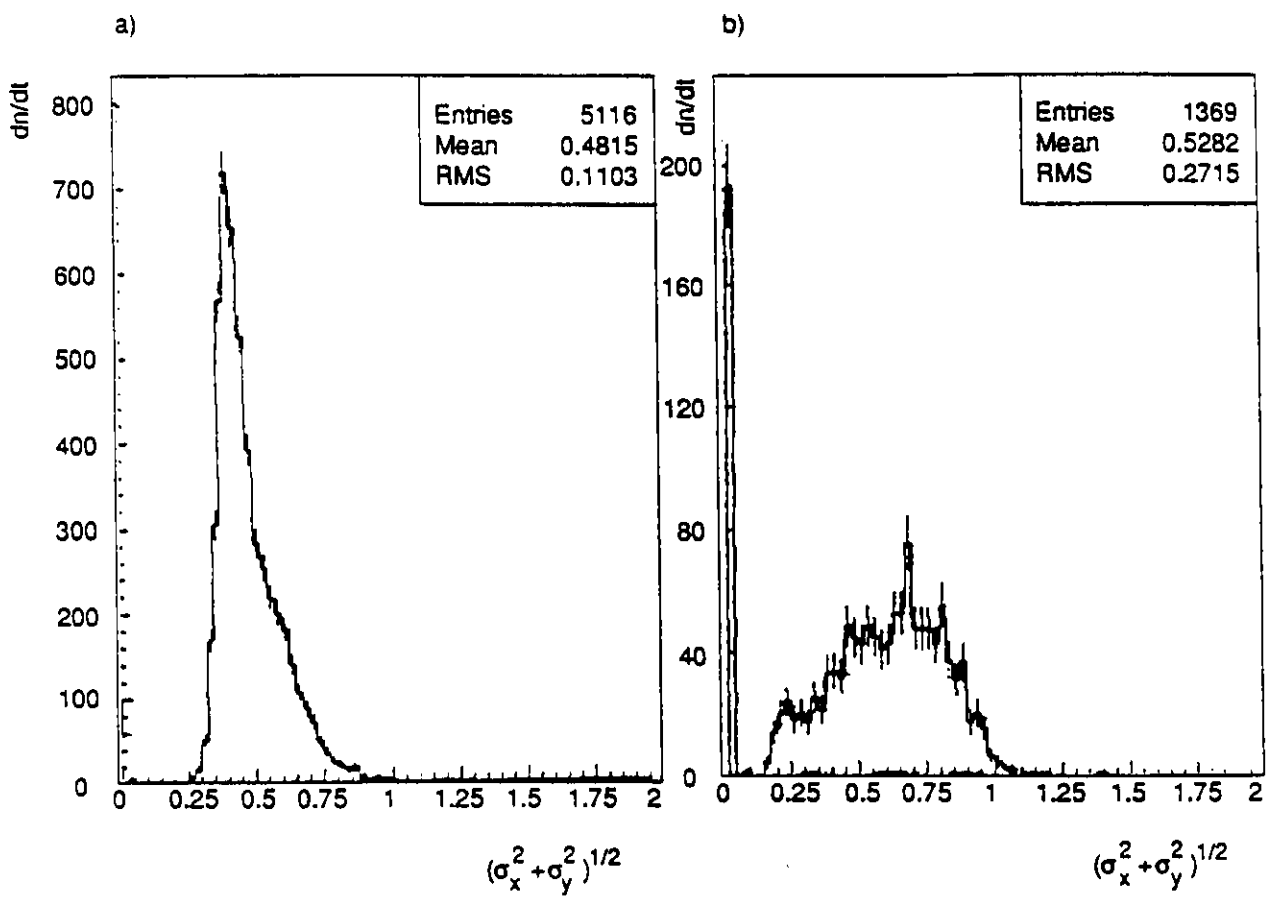Figure 11:

Figure 12:

24

a)

Entries 6129
Mean   35.22
RMS   14.16

b)

Entries 6129
Mean   40.69
RMS   15.03

Figure 13:

25

a)

b)

	Entries	5116
Mean		0.4815
RMS		0.1103

	Entries	1369
Mean		0.5282
RMS		0.2715

$(\sigma_x^2 + \sigma_y^2)^{1/2}$

$(\sigma_x^2 + \sigma_y^2)^{1/2}$
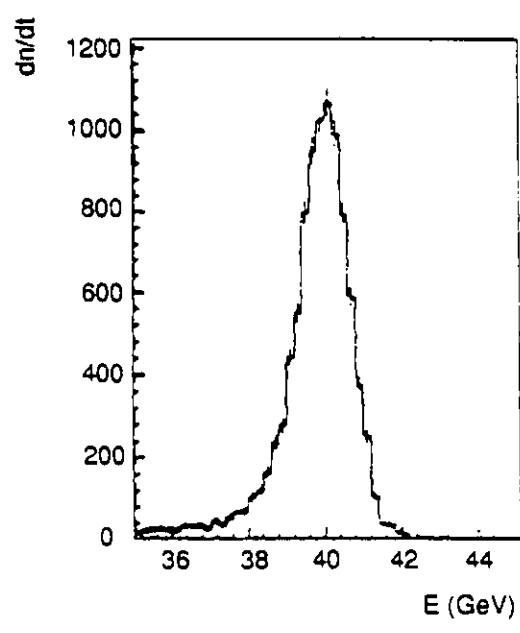
Figure 14:

Figure 15:

Figure 16:

27